Environmental Science Nano

ROYAL SOCIETY OF CHEMISTRY

PAPER

View Article Online
View Journal

Cite this: DOI: 10.1039/d4en00884g

A portable and reusable sensor system based on graphene for real-time and sensitive detection of lead ions in water†

Byunghoon Ryu,‡[ab] Wen Zhuang,‡[ac] Hyun-June Jang,[ac] Zhenwei Gao,[ac] Yuqin Wang[ac] and Junhong Chen *[ac]

Received 22nd September 2024,
Accepted 22nd December 2024

DOI: 10.1039/d4en00884g

rsc.li/es-nano

Long-term exposure to Pb^{2+} can cause irreversible damage to the nervous, cardiovascular, and reproductive systems. Therefore, developing a fast and sensitive detection system capable of monitoring minuscule concentrations of Pb^{2+} is essential. In this study, we demonstrated a fully portable sensor system enabling rapid, sensitive, and real-time monitoring of Pb^{2+}. The sensor system adopted the remote-gate field-effect transistor (RGFET) detection scheme and was easy to operate, even for non-experts. The sensor system comprised two printed circuit boards (PCBs): a sensor PCB with a remote-gate electrode and an analyzer PCB with a metal-oxide-semiconductor field-effect transistor (MOSFET) transducer and peripheral electronics to manage sensor signals. To achieve a high sensitivity for Pb^{2+}, we utilized graphene ink drop-casted on the sensor PCB as a sensing membrane. The graphene film was easy to deposit and remove, enabling the sensor PCB to be reused multiple times. The sensor system was further linked to a smartphone application that instantly monitors the sensor response, allowing for rapid point-of-use detection. The sensor exhibited a high sensitivity of 21.7% when the limit of detection (LOD) value of 1 nM (~0.2 ppb) was detected, and the typical detection time for each sample was approximately 60 seconds. This portable sensor system advances sensing technologies and could potentially supplement expensive, laborious conventional sensing equipment.

Environmental significance

Environmental exposure to Pb^{2+} poses significant risks to humans and ecosystems, underscoring the need for a rapid and sensitive detection system for trace concentrations of Pb^{2+} in water. Traditional methods for Pb^{2+} detection are often costly, complicated, and time-consuming and thus are insufficient for real-time *in situ* monitoring. In this study, we present a fully portable sensor system based on field-effect transistor (FET) technology that enables rapid, sensitive, and real-time detection of Pb^{2+}. The sensor exhibits an ultra-low detection limit of 1 nM (~0.2 ppb) and features a graphene-ink-based gate electrode that can be recycled for repeated tests. This electronic sensing advancement is significant for water quality testing and offers substantial benefits for environmental monitoring.

1. Introduction

The U.S. Environmental Protection Agency (EPA) defines the maximum contaminant level (MCL) of lead ions (Pb^{2+}) in drinking water as 15 ppb.[1] However, there is no safe level of lead in drinking water because prolonged exposure to Pb^{2+} can lead to its accumulation in the human body over time, thereby resulting in critical impairment of the nervous, cardiovascular, and reproductive systems.[2,3] Therefore, developing a detection system that can rapidly and sensitively monitor minuscule levels of Pb^{2+} in water is imperative to enable diagnostic and restorative measures for preventing long-term damages. However, current prevailing methods, such as inductively coupled plasma mass spectrometry (ICP-MS),[4] atomic fluorescence spectroscopy,[5] and atomic absorption spectroscopy,[6] cannot meet these requirements, as they need expensive instruments with operational expertise and time-consuming sample delivery, which prevents timely monitoring of toxic Pb^{2+}.

To tackle the above-mentioned challenges, several attempts to develop portable sensors facilitating rapid and sensitive detection of Pb^{2+} have been reported.[7–11] Yap *et al.*[10] developed a handheld microfiber-based sensor for detecting

[a] *Chemical Sciences and Engineering Division, Physical Sciences and Engineering Directorate, Argonne National Laboratory, Lemont, Illinois 60439, USA. E-mail: junhongchen@anl.gov*
[b] *Department of Mechanical Engineering, Inha University, Incheon, 22212, Republic of Korea*
[c] *Pritzker School of Molecular Engineering, University of Chicago, Chicago, Illinois 60637, USA. E-mail: junhongchen@uchicago.edu*

† Electronic supplementary information (ESI) available. See DOI: https://doi.org/10.1039/d4en00884g

‡ B. R. and W. Z. contributed equally to this work.

optical signal changes related to the concentration of Pb^{2+} around the microfiber. Particularly, the surface of the fiber was functionalized with L-glutathione (GSH) receptors, altering the effective refractive index upon binding with Pb^{2+}, which resulted in a red shift of the output transmission spectrum of the incident light traveling through the fiber. The limit of detection (LOD) of this sensor was ~5 ppb, and the typical detection time was ~4 min for each pre-prepared sample. Huang *et al.*[7] adopted a commercial electronic balance as a readout device precisely measuring the weight of the overflowed water, which is associated with the concentration of Pb^{2+}. More specifically, the activation of DNAzyme occurred in the presence of Pb^{2+}, which released hybridized platinum nanoparticles (PtNPs), subsequently triggering the catalytic reaction with hydrogen peroxide (H_2O_2) in a sealed glass bottle equipped with a drainage tube. Therefore, the water drained out of the tube because the pressure in the sealed bottle increased due to the formation of oxygen gas. This detection approach took ~60 min for each detection cycle, and the LOD was ~0.83 nM (~0.17 ppb). Similarly, Jiang *et al.*[8] employed DNAzyme to build a portable detection scheme for Pb^{2+}. In this scheme, the DNAzyme detained a crosslinker substrate for the hydrogel, releasing the substrate once Pb^{2+} formed, which induced the phase transition of the hydrogel from a gel to a solution. Eventually, the solution phase of the hydrogel ascended a capillary channel, whose height was measured as a sensor response. The detection time and LOD were ~1 h and 10 nM (~2 ppb), respectively. Despite such encouraging progress in developing portable Pb^{2+} sensors, there remain unmet technical voids because they are either still hard to operate for novices or are not fully portable, requiring additional analyzers.

Meanwhile, field-effect transistor (FET) sensors have been extensively studied for lead ion detection[12–15] owing to their distinct advantages such as rapid response, ultralow detection limits and direct digital readouts. Among these FET sensors, remote-gate (extended-gate) FET devices have emerged as promising candidates due to their enhanced operational stability,[16–19] which benefits from the structural isolation of the semiconductor channel of the FET from the solution-contacting sensing area. Despite their impressive performance, critical challenges remain in manufacture scalability, device reusability and circuit integration, which may limit their practical applications in portable systems.

Herein, we report a fully portable sensor system that enables rapid, sensitive, and real-time monitoring of Pb^{2+} as well as is easy to operate even for a layperson based upon the remote-gate field-effect transistor (RGFET) detection scheme known for high detection stability and reliability.[18,19] The portable sensor consists of a sensor printed circuit board (PCB) and an analyzer PCB corresponding to a remote gate and an n-type metal-oxide-semiconductor field-effect transistor (MOSFET) transducer of the RGFET, respectively. In particular, we made use of graphene ink drop-casted on top of the sensor PCB as a sensing membrane, achieving high sensitivity toward Pb^{2+} due to the high surface-to-volume ratio and electrical conductivity of the graphene nanoflakes.[20,21] Furthermore, the Cu-plated surface of the sensor PCB provides adequate adhesion to the graphene ink, allowing facile deposition and removal, which results in the ability to reuse the sensor PCB repeatedly. Interfacing with a smartphone application to instantaneously visualize the sensor response, the portable sensor system exhibits a high sensitivity of 21.7% when detecting its LOD value of 1 nM (~0.2 ppb), and the typical detection time for each sample is 60 seconds. Such a portable sensor could be further developed into a reliable detection system supplementing expensive and labor-intensive conventional sensing instruments.

2. Experimental method

2.1. Designing the analyzer PCB of the portable sensor system

First, a 32-bit microcontroller (MCU, Seeed Xiao) was chosen to control peripheral electronics manipulating and transmitting sensor signals. To generate and supply a precisely adjusted reference voltage (2.054 V) to a reference electrode (BASi, MW-2021), a shunt voltage reference (LM4040) was integrated into the analyzer PCB. When the surface potential was delivered from the sensor PCB to the gate pin of the MOSFET (CD4007), the drain current flowed into a resistor connected to the drain pin of the n-type MOSFET, which converted the drain current to voltage-type sensor signals. Such sensor signals traveled to a 16-bit analog-to-digital chip (AD1115) and were then were digitized, enabling a readout from the MCU. The sensor signals were further delivered to a smartphone app through a Bluetooth module (HM-10) or displayed on an OLED panel.

2.2. Functionalizing the sensor PCB of the portable sensor system

Before functionalization, graphene ink (Sigma-Aldrich, 793663, 2.4 wt% graphene nanoflakes) was diluted with the background solvent consisting of 85% cyclohexanone (Sigma-Aldrich, 398241) and 15% terpineol (Sigma-Aldrich, 86480). The as-prepared graphene ink was deposited onto the Cu-plated electrode pad of the sensor PCB *via* drop casting and post-annealed using a horizontal furnace for 30 min in an argon gas environment at 250 °C. Then, 1-pyrenebutyric acid (PBA) (TCI, P1213) was dissolved in dimethylformamide (DMF) (Sigma-Aldrich, 319937) to prepare a 10 mM solution. Next, a droplet (3 μL) of the PBA solution was pipetted onto the graphene film and incubated in a closed chamber for 1.5 h. The functionalized graphene film was washed with DMF three times to remove unbound PBA and dried with nitrogen gas for sensor measurements.

2.3. Sensor measurement and operation

Pb^{2+} solutions were prepared by dissolving $PbCl_2$ powder (Sigma-Aldrich, 268690) in deionized water or tap water and diluted to targeted concentrations. For selectivity tests, the interference solutions were prepared similarly with $CuCl_2$

(Sigma-Aldrich, 459097), $ZnCl_2$ (Sigma-Aldrich, 429430), $FeCl_3$ (Sigma-Aldrich, 157740), $NiCl_2$ (Sigma-Aldrich, 654507), $MnCl_2$ (Sigma-Aldrich, 244589), $CaCl_2$ (Sigma-Aldrich, 223506), $MgCl_2$ (Sigma-Aldrich, 255777), and NaCl (Sigma-Aldrich, S7653), respectively. A 15 μL testing solution prepared above was pipetted onto the sensor PCB. An Ag/AgCl reference electrode contacted the testing solution in order to apply the gate bias for all the measurements. An n-type MOSFET (CD4007) was connected with the sensor PCB as a transducer and used for all measurements consistently. All the transfer curves were measured by a Keithley 4200A semiconductor analyzer with drain voltage set at 50 mV. Each testing solution was then removed by pipetting after each round of measurement. The threshold voltage was calculated as the gate voltage corresponding to a drain current of 1 μA in each transfer curve, and the average signal changes were calculated based on the results from three measurements. The smartphone application was designed using Android Studio. Each detection curve, after finishing the measurement, was extracted in the ASCII format and sent to email or messenger applications.

3. Results and discussion

3.1. Strategies to design a portable RGFET sensor

RGFET offers plenty of benefits in sensing applications, such as fast response, high sensitivity, and detection stability.[18,19] In particular, stability is a favorable characteristic hard to expect from numerous other nano-sensors, making the RGFET likely to be further developed into a miniaturized, portable and commercial sensor. Such stability of the RGFET is attributed to its device structure formulated by the equation below.[16]

$$V_{th} = V_{th\_FET} + E_{ref} + \phi_{lj} - \varphi_s + \chi_{sol} + \frac{\phi_G}{q} \quad (1)$$

where V_{th} and V_{th_FET} are threshold voltages of the RGFET and its component, MOSFET, respectively, E_{ref} is the standard potential of an Ag/AgCl reference electrode (+0.209 V *vs.* NHE, BASi Corp.), ϕ_{lj}, φ_s, and χ_{sol} are potentials associated with the liquid junction, sensing membrane, and solution interfaces, and ϕ_G is the work function of graphene. According to eqn (1), the change in the threshold voltage of the RGFET, V_{th}, only depends on events at the surface of the sensing membrane because V_{th_FET} and E_{ref} are stable variables derived from a commercial MOSFET and the reference electrode, respectively. Therefore, the RGFET exhibits high detection stability when it operates with the optimized sensing membrane and protocols.

Fig. 1 schematically shows the graphene RGFET consisting of a remote gate and a MOSFET, which requires a bulky device setup for the detection test. In conventional operation, the transfer characteristic curves of the RGFET are measured repeatedly by a skilled operator as various concentrations of analytes are introduced into the sensing membrane. Subsequently, additional post-processes need to be done to accurately extract the sensor responses, ΔV_{th}, associated with the concentration of the analytes, which is time-consuming and far from real-time detection, as shown in Fig. 1(c). To achieve facile and real-time detection capability, it is more reasonable to capture another sensor response of the RGFET, I_{DS}, continuously and directly correlate those with the concentrations of analytes, as shown in Fig. 1(d). ΔV_{th} and ΔI_{ds} are both derived features from the shifts of FET transfer curves, while ΔI_{ds} signals are amplified by the field effect and more accessible for circuit integration. Along with such a modified sensor operation approach, the RGFET, including a bulky and expensive analyzer, is necessarily miniaturized to develop a portable sensor. Specifically, the remote gate shown in Fig. 1(a) and the MOSFET and analyzer shown in Fig. 1(b) are preferably designed into a sensor PCB and an analyzer

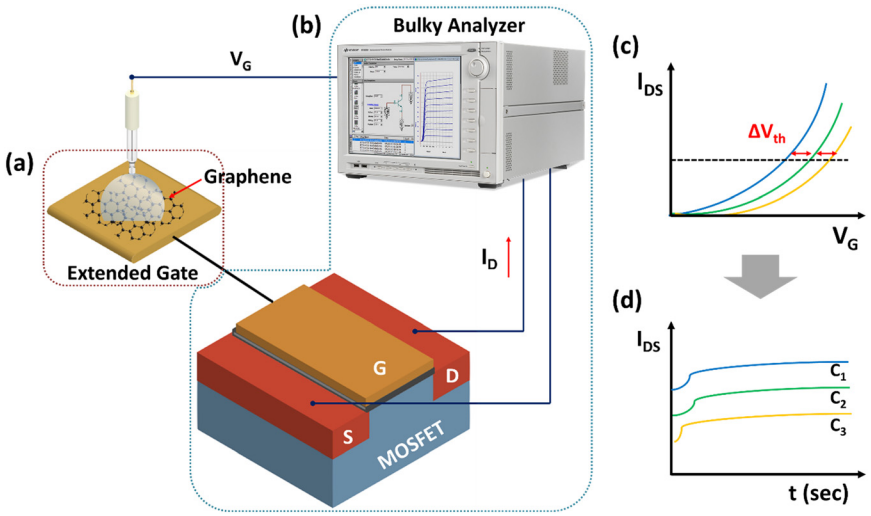

Fig. 1 Conventional setup for operating a remote-gate graphene sensor. (a) A remote gate separated from a MOSFET transducer. (b) A transducer and an analyzer for acquiring sensor signals. (c) Transfer characteristic curves observed in typical operation. (d) Real-time monitoring of I_{DS} for portable sensor operation.

PCB, respectively. Considering these strategies, it is feasible to reduce the size of the conventional RGFET sensor and make it portable, in addition to having high sensitivity, stability, and real-time monitoring capability.

3.2. The sensor PCB design and deposition of graphene

As a first step, the remote gate of the RGFET was replaced with the sensor PCB shown in Fig. 2(a). The sensor PCB had a miniaturized size of 38 mm × 18 mm consisting of a circular electrode pad, which is a substrate for the graphene sensing membrane, and a USB connector prepared for facile connection with the analyzer PCB. The diameter of the exposed pad was designed to be 5 mm, which made it more convenient to deposit the graphene film since the whole region of the pad was easily covered by the drop-casting of a single droplet of graphene ink (1.5 μL). Fig. 2(b) shows graphene films deposited on the pad using various concentrations of ink to optimize the thickness of graphene. A commercially available graphene ink was purchased from Sigma-Aldrich (Product No. 793663) and sequentially diluted three times in each step by adding its background solvent (cyclohexanone/terpineol). Initially, all four graphene ink droplets occupied the entire pad surface but eventually resulted in different coverages of graphene films after drying and annealing. Specifically, the graphene ink diluted three times produces a full-coverage film while further diluted inks led to low-coverage films. The thickness of the graphene films was evaluated *via* cross-sectional scanning electron microscopy (SEM) (Fig. S1†), and Fig. 2(c) shows thickness profiles obtained from the full-coverage films formed using pristine and 3× diluted inks. The thickness of the film produced using the 3× diluted ink was ~0.91 μm, which was ~76% thinner than that produced using the pristine ink (~3.89 μm). It should be noted that thin graphene film is beneficial because the thinner film is prone to forming a stable interfacial contact with the electrode pad. Therefore, the thinner one out of the two full-coverage graphene films was chosen for the sensing membrane of the portable sensor. Fig. 2(d) displays a scanning electron microscopy (SEM) image of the thin graphene film. Graphene nanoflakes are evenly stacked, completely covering the electrode pad with no vacant areas. Lastly, Fig. 2(e) compares the resistivity of the film before and after the annealing process. The commercial graphene ink used in this study contained ethyl cellulose as a dispersant, degrading the graphene film's electrical conductivity, but it was removable at high temperatures of about ~300 °C. After annealing, the resistivity of the graphene film was significantly reduced to ~220 mΩ cm. Such a low resistivity of the film is in good agreement with previously reported values, making it a suitable sensing membrane.[22]

3.3. Pb^{2+} detection using the sensor PCB with graphene films

To verify the detection capability toward Pb^{2+}, two sensor PCBs with deposited graphene films using pristine and 3× diluted inks were prepared, as shown in Fig. 3(a). Here, the sensor PCB holding a thin graphene film is distinctively noticeable because the reddish color pattern on the film originates from the thin-film interference. Before the detection test, both sensor PCBs were functionalized using

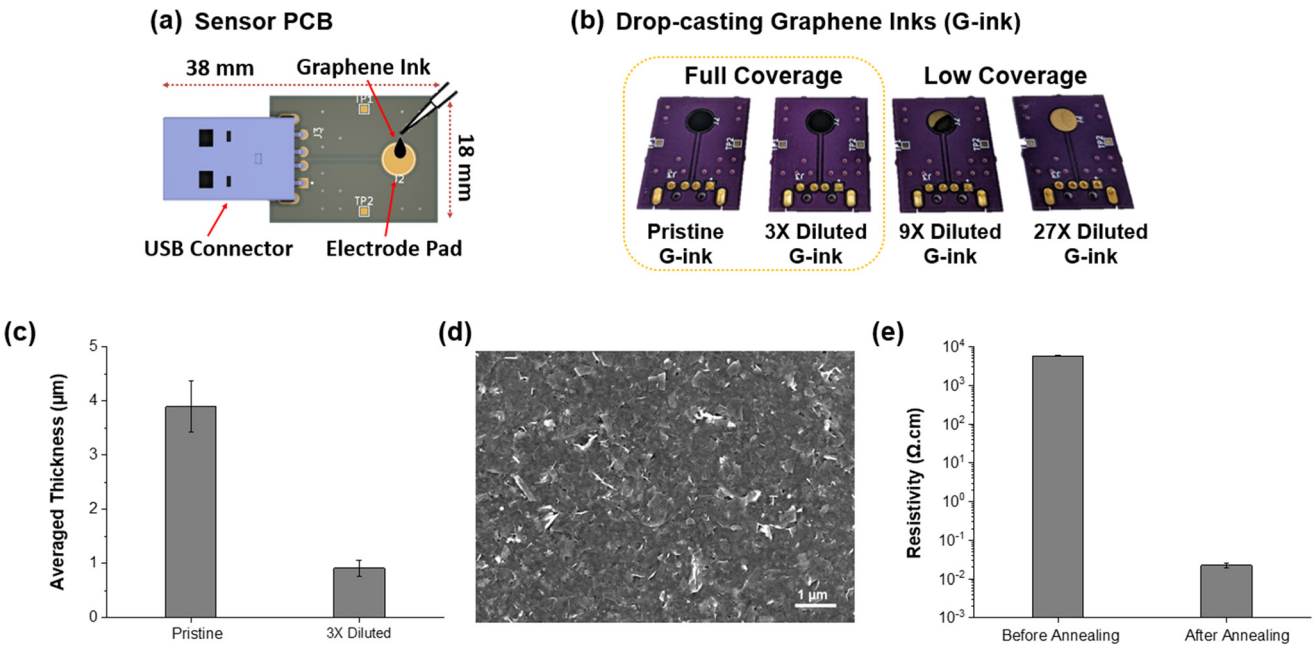

Fig. 2 A sensor PCB replacing the conventional remote gate. (a) A schematic of the sensor PCB including a USB connector for facile connection to an analyzer PCB. (b) Optimization of graphene ink deposition onto the electrode pad. (c) Thickness profiles obtained from the films formed using pristine and 3× diluted inks. (d) An SEM image of the film deposited using 3× diluted graphene ink. (e) Comparison of electrical resistivity of the graphene film prepared by 3× diluted ink before and after the annealing process.

1-pyrenebutyric acid (PBA) conjugated with graphene nanoflakes *via* π–π interactions, as depicted in Fig. 3(b). Fig. S2† shows the contact angle profiles of the prepared thin films and reveals that the surface hydrophilicity significantly increases after surface functionalization, suggesting the successful conjugation of PBA probes on the graphene surface. PBA is responsible for the sensitive and selective detection of Pb^{2+} because it bears the carboxylic acid end group, which induces a chelation reaction with Pb^{2+} ions, resulting in lead carboxylates.[23] Chelation significantly changes the electric double-layer (EDL) and thus alters the surface potential of the electrode,[24] which leads to the shift of the FET transfer curve. As the concentration of lead ions increased, the shift of the transfer curve increased until reaching the saturation point. It is worth noting that graphene films on the sensor PCBs remained intact despite prolonged exposure to an aqueous environment during the functionalization process. This is attributed to the relatively rough surface of the Cu-plated electrode pad, as shown in Fig. S3,† which provides sufficient adhesion to prevent the films from delamination. Fig. 3(c) shows the detection setup for Pb^{2+}, including a commercial MOSFET (CD4007), an Ag/AgCl reference electrode (MW-2021), and a semiconductor analyzer. The reference electrode is in contact with a water solution containing Pb^{2+}, and supplies the sweeping voltage to the sensor PCB. Afterward, altered surface potential owing to the binding reactions is transmitted to the gate of the MOSFET, which modulates its transfer characteristics. Fig. 3(d) plots the shift in the transfer characteristic curves with respect to the concentration of Pb^{2+} measured using the sensor PCB with a thin graphene film. As a comparison, a plot of transfer curves obtained using the sensor PCB with a thick graphene film is shown in Fig. S4.† Each transfer curve was acquired after 5 min incubation per Pb^{2+} solution droplet. Subsequently, the threshold voltage, V_{th}, of each curve was captured by investigating intersects when extending the horizontal line at I_{DS} = 1 μA and serves as a sensor response (R). With increasing concentration of Pb^{2+}, threshold voltages increased accordingly, attributed to the formation of lead carboxylates, which repel electrons and deplete the semiconductor channel of the n-type MOSFET.[25,26] Fig. 3(e) compares the changes in threshold voltage *vs.* Pb^{2+} concentrations using two sensor PCBs composed of thick and thin graphene films. The sensor responses, V_{th}, obtained from both sensor PCBs are directly proportional to the logarithm of concentrations, which demonstrates the sensor's ability to detect Pb^{2+}. The sensitivity of the sensor, defined as the relative change in sensor responses ($(R_i - R_0)/R_0 \times 100\%$), is further calculated and displayed in Fig. 3(f). The sensitivity toward Pb^{2+} detection using the sensor PCB with the thin graphene film is about 10-fold higher than that of the sensor PCB with the thick graphene film, attributed to the fact that the thin graphene film could form a more stable electrical connection to the electrode pad, which results in the effective

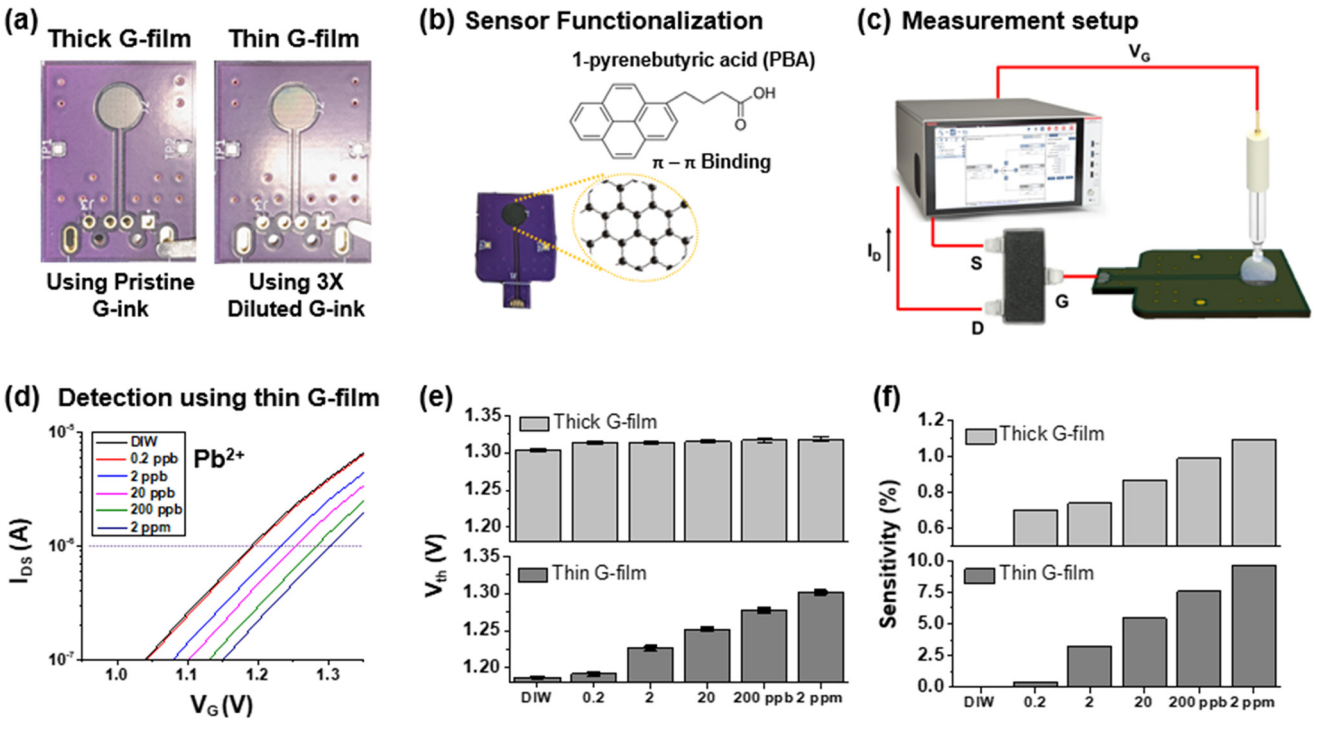

Fig. 3 Lead ion detection using the sensor PCB drop-casted by the graphene film (G-film). (a) Sensor PCBs bearing thick and thin G-films, deposited using pristine and 3× diluted G-inks, respectively. (b) Functionalization of the sensor PCBs for lead ion detection. (c) Detection setup using the sensor PCB, MOSFET, and analyzer. (d) Transfer curves of the MOSFET upon detection of lead ions ranging from 0.2 ppb to 2 ppb using thin G-film sensor. (e) and (f) Changes in threshold voltages (V_{th}) and sensitivity (%) with respect to lead ion concentrations using both thick and thin G-film sensors.

transfer of the surface potential change to the MOSFET.[27] As a result of these comparative tests, it was decided to use a thin layer of graphene as a sensitive sensing membrane to develop the portable sensor.

3.4. Selectivity and reusability of the sensor PCB

The selectivity and reusability of the sensor PCB containing the thin graphene film were additionally evaluated. Fig. 4(a) shows the sensitivity of the sensor toward major interfering cations in municipal water at a concentration of 100 nM (*i.e.*, 20 ppb). Notably, Pb^{2+} elicits the most pronounced response, with a sensitivity approximately ten-fold greater than that of the other ions, which underscores the sensor's selectivity toward Pb^{2+}. The selectivity is likely attributed to lead ions having much stronger affinity toward carboxylic groups to form complexes compared to other cations.[28] An important advantage of the sensor PCB worth highlighting is its ability to be reused multiple times. Specifically, the graphene film deposited on the sensor PCB can be readily removed once detection is completed through a straightforward wiping process using an alcohol wipe, as shown in Fig. S5.† Subsequently, the sensor PCB can be refreshed for the following assay *via* drop-casting of fresh graphene ink. Fig. 4(b) describes the refreshing process and the reusability of the sensor PCB. To demonstrate the reusability, detection tests for Pb^{2+} were repeatedly conducted while the sensor PCB was refreshed three times. The sensor response plot in Fig. 4(b) indicates no significant degradation in the threshold voltages for every Pb^{2+} concentration despite the sensor PCB being repeatedly used, thus confirming its reusability.

3.5. Design of the fully portable sensor system

Fig. 5(a) shows the schematic design of an analyzer PCB capable of substituting the bulky and expensive commercial analyzer to be assembled with the sensor PCB to construct the portable sensor system. The analyzer PCB consisted of a series of electrical components, including an operational amplifier, a 16-bit analog-to-digital converter, and a Bluetooth module for amplifying, digitizing, and transferring sensor signals. Particularly, the footprint of the PCB was 43 mm × 30 mm, powered by a tiny 3.7 V LiPo battery, which guaranteed its excellent portability. A detailed circuit diagram of the analyzer PCB is presented in Fig. S6.† In operation, the analyzer PCB delivered precisely regulated voltage to the sensor PCB *via* the reference electrode, resulting in the drain current (I_{DS}) of the MOSFET. Fig. S7† shows the drain current as a function of the gate and drain voltage for the MOSFET (CD4007). Such a time-dependent drain current associated with the concentration of Pb^{2+} was subsequently converted to the voltage, amplified, and wirelessly transmitted to a smartphone using the Bluetooth module. Fig. 5(b) displays the assembly of the sensor and analyzer PCBs and a prototype designed by packaging them. It is worth noting that the assembly process of PCBs can be accomplished with ease through a pair of standard USB connectors. Moreover, the overall dimensions of the prototype were 60 mm (L) × 40 mm (W) × 50 mm (H), making it both compact and portable. The sensor signals from the prototype can be transmitted to a smartphone application to facilitate prompt and real-time monitoring, as shown in Fig. 5(c). The smartphone application integrates a calibration equation to exhibit the concentrations of Pb^{2+} and plot their variation over time. Upon exceeding the EPA's MCL for Pb^{2+} in water, the application notifies the user of the potential hazard through a visible alarm.

3.6. Pb^{2+} detection using the portable sensor

Fig. 6 shows the efficacy of the portable sensor system in Pb^{2+} detection. Fig. 6(a) presents a real-time plot showcasing the detection of various concentrations of Pb^{2+}. After switching on the sensor, there was an upsurge in sensor signals as the sample solutions are introduced after about 20 seconds. A decrease in the sensor signal was observed with an increase in the concentration of Pb^{2+}, attributed to the formation of lead carboxylates, which reduced the drain current of the MOSFET. It is worth mentioning that the sensor signals become steady within 60 seconds of initiating measurement, enabling the sensor to detect Pb^{2+} rapidly. The sensitivity of the sensor was calculated using the sensor signals recorded at 60 seconds, as illustrated in Fig. 6(b). The overall sensitivity of the portable sensor was noticeably high, surpassing 20% at all concentrations. This is attributed to its working principle for measuring I_{DS} that provides high response toward Pb^{2+} detection and the signal amplification

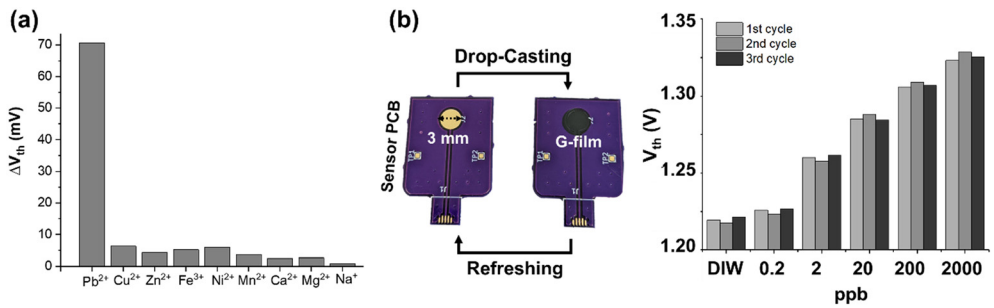

Fig. 4 Selectivity and reusability of the graphene sensor. (a) Sensor responses toward various metal ions with a concentration of 100 nM. (b) A process to refresh the sensor PCB and lead ion detection using the same graphene sensor PCB recycled three times.

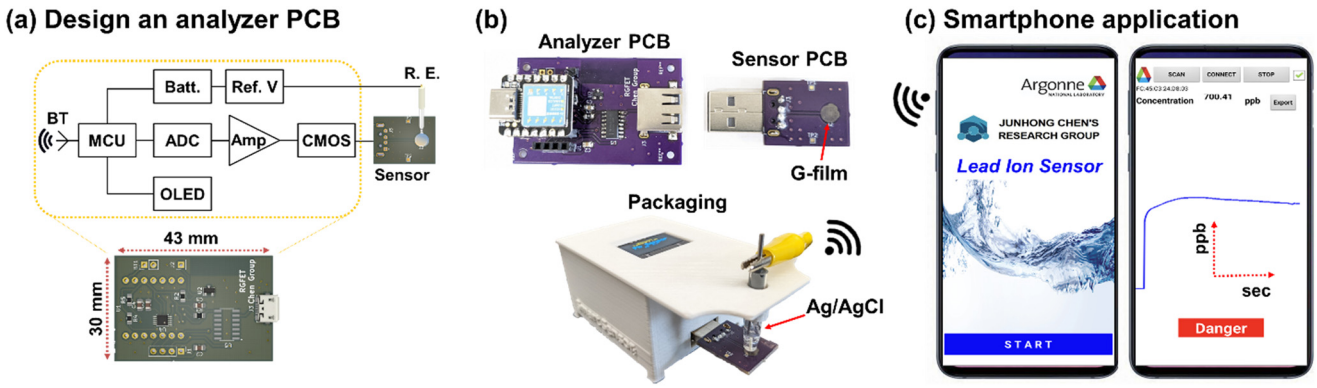

Fig. 5 A portable sensor system for the real-time monitoring of lead ions in drinking water. (a) A schematic of the analyzer PCB. (b) A prototype of the portable sensor including the analyzer and sensor PCBs. (c) A wireless communication capability of the portable sensor system with a smartphone application.

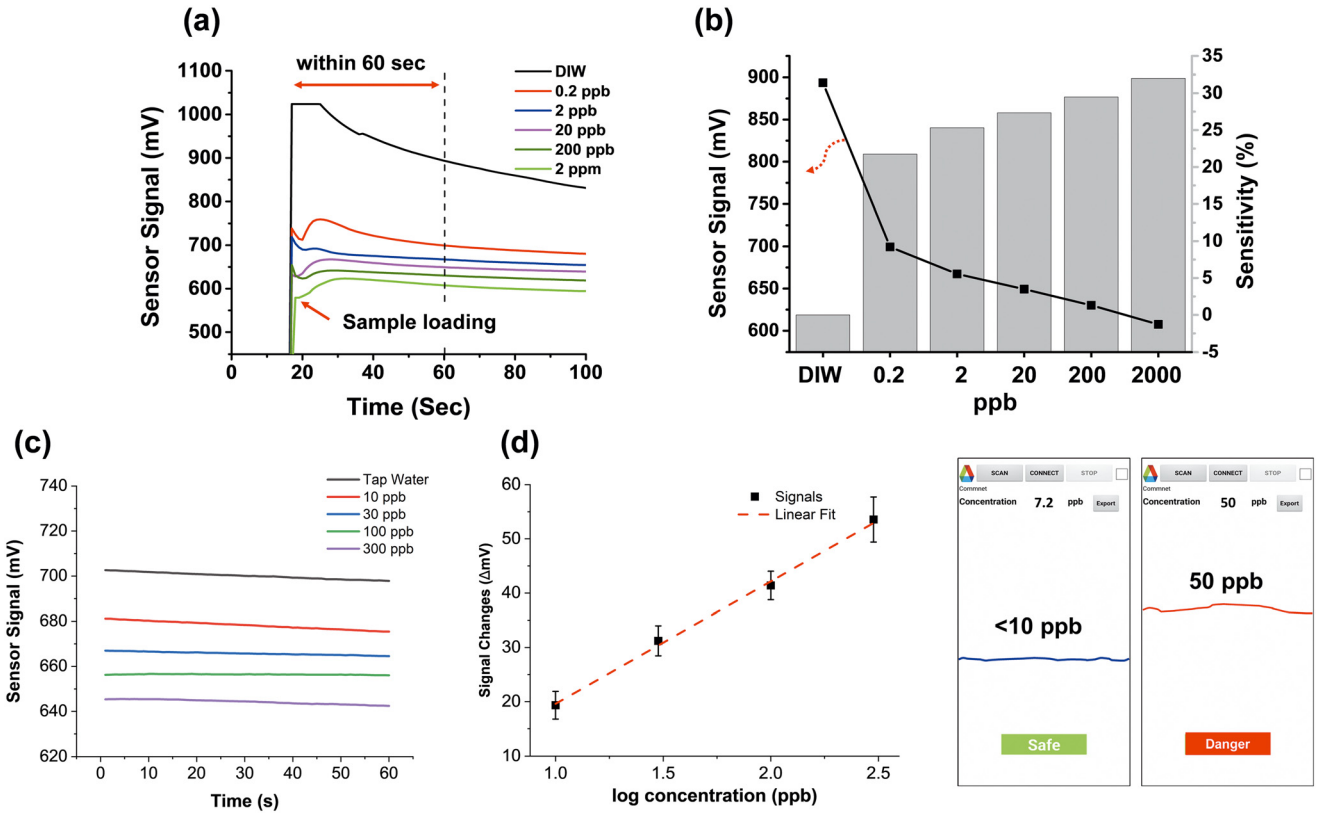

Fig. 6 Lead ion detection using the portable sensor system. (a) A real-time detection plot as a function of lead ion concentrations. (b) Sensitivity of the portable sensor system toward the lead ion, calculated using the relative change in sensor signals captured at 60 seconds from (a). (c) Real-time detection of lead ions spiked in tap water. (d) A calibration plot of the portable sensor system and the ability to detect the toxic lead ions in tap water using the smartphone application.

circuit integrated into the analyzer PCB. In particular, the sensor's sensitivity remained impressive, with a value of 21.7%, when measuring a low concentration of Pb^{2+} at 1 nM (*i.e.*, 0.2 ppb), which remained high compared to the sensitivity of other portable sensors previously reported. To provide a more comprehensive comparison, we present in Table 1 the critical characteristics of our portable sensor alongside those of other sensors utilized for Pb^{2+} detection.[7–11] Fig. S8† demonstrates further assessment of the portable sensor's ability to detect Pb^{2+} through the utilization of a sensor PCB containing a thick graphene film, leading to a much lower sensitivity.

The detection ability of the portable sensor in tap water spiked with Pb^{2+} was further assessed, as shown in Fig. 6(c). To mimic the Pb^{2+}-contaminated tap water samples, test samples were prepared by spiking $PbCl_2$ salts into lead-free tap water at

Table 1 Comparison of portable sensors for lead ion detection

Detection method	Sensitivity	LOD	Detection time	Note	Ref.
DNAzyme-based biosensor on a portable optic fiber	~10.3% (@ 0.2 ppb)	0.2 ppb (1.03 nM)	10 min	Require a bulky fluorescent analyzer	11
DNAzyme-based visual capillary sensor	~1900% (@ 2 ppb)	2 ppb (10 nM)	1 h	Require a ruler to measure the capillary distance	8
Handheld microfiber-based sensor	~0.06% (@ 10 ppb)	5 ppb (~24 nM)	4 min	Size of the whole system 203 × 149 × 65 mm	10
DNAzyme-based sensor using electronic balance as a readout device	~64.8% (@ 5 ppb)	0.17 ppb (0.83 nM)	60 min	Require skilled operators and an expensive balance	7
Ion-responsive photonic hydrogel sensor	~4.34% (@ 100 ppm)	200 ppb (1 μM)	180 min	Require a fiber optical spectrometer	9
Graphene on a portable RGFET sensor	21.7% (@ 0.2 ppb)	0.2 ppb (1 nM)	60 s	Small size of the whole system (60 × 40 × 50 mm)	This work

varying concentrations (10, 30, 100 and 300 ppb). The portable sensor exhibited a high sensitivity in all the test samples, even at the lowest concentration of 10 ppb, which is below the EPA action level/MCL (15 ppb). The calibration plot depicted in Fig. 6(d) was generated by processing and fitting multiple test results. The resulting calibration equation was extracted from the plot and subsequently integrated into the portable sensor system. Consequently, such an integration allowed the sensor to provide timely warnings regarding the presence of toxic Pb^{2+} levels in tap water *via* the smartphone application.

4. Conclusion

In conclusion, we have developed and presented a fully portable sensor system for the rapid, sensitive, and real-time monitoring of Pb^{2+}. The sensor is based on the RGFET detection scheme and is easy to operate even for those without specialized training. The portable sensor consists of two PCBs: a sensor PCB with a remote gate and an analyzer PCB including a MOSFET transducer and peripheral electronics for handling sensor signals. To achieve a high sensitivity toward Pb^{2+}, graphene ink drop-casted on top of the sensor PCB was used as a sensing membrane. Such a graphene film was facile to deposit and remove, thereby allowing for the reuse of the sensor PCB multiple times. The portable sensor system was interfaced with a smartphone application that instantaneously monitors the sensor response, enabling rapid point-of-use detection. This portable sensor system can be a reliable, cost-effective supplement for expensive, labor-intensive conventional sensing instruments. Overall, the development of this portable sensor represents a significant advance in the field of sensing technologies as it provides a fast and sensitive approach for detecting Pb^{2+} in real-time, which could ultimately benefit various practical applications, including environmental monitoring and medical diagnosis.

Data availability

The authors declare that the data supporting the findings of this study are available in the paper and its ESI† files. If raw data files in another format are needed, they can be obtained from the corresponding author upon reasonable request.

Conflicts of interest

J. C. is a founder and consultant of NanoAffix Science LLC. NanoAffix did not fund the research reported here.

Acknowledgements

B. R. acknowledges the support from the National Research Foundation of Korea (NRF) grant funded by the Korean Government (MSIT) (RS-2023-00247462) and the Inha University Research Grant. W. Z. acknowledges the support from an NRT grant from the National Science Foundation (Grant No. 2022023).

References

1 US Environmental Protection Agency, *Control of lead and copper*, Electronic Code of Federal Regulations, 2020.
2 R. L. Canfield, C. R. Henderson Jr, D. A. Cory-Slechta, C. Cox, T. A. Jusko and B. P. Lanphear, Intellectual impairment in children with blood lead concentrations below 10 μg per deciliter, *N. Engl. J. Med.*, 2003, **348**(16), 1517–1526.
3 M. Edwards, Fetal death and reduced birth rates associated with exposure to lead-contaminated drinking water, *Environ. Sci. Technol.*, 2014, **48**(1), 739–746.
4 L. Balcaen, E. Bolea-Fernandez, M. Resano and F. Vanhaecke, Inductively coupled plasma–Tandem mass spectrometry (ICP-MS/MS): A powerful and universal tool for the interference-free determination of (ultra) trace elements–A tutorial review, *Anal. Chim. Acta*, 2015, **894**, 7–19.
5 I. B. Karadjova, L. Lampugnani, A. D'Ulivo, M. Onor and D. L. Tsalev, Determination of lead in wine by hydride generation atomic fluorescence spectrometry in the presence of hexacyanoferrate (III), *Anal. Bioanal. Chem.*, 2007, **388**, 801–807.
6 M. Ghaedi, F. Ahmadi and A. Shokrollahi, Simultaneous preconcentration and determination of copper, nickel, cobalt and lead ions content by flame atomic absorption spectrometry, *J. Hazard. Mater.*, 2007, **142**(1–2), 272–278.

7 Y. Huang, C. Lin, F. Luo, B. Qiu, L. Guo, Z. Lin and G. Chen, Ultrasensitive and portable assay for lead (II) ions by electronic balance as a readout, *ACS Sens.*, 2019, **4**(9), 2465–2470.
8 C. Jiang, Y. Li, H. Wang, D. Chen and Y. Wen, A portable visual capillary sensor based on functional DNA crosslinked hydrogel for point-of-care detection of lead ion, *Sens. Actuators, B*, 2020, **307**, 127625.
9 Z. Peng, H. R. Yu, J. Y. Wen, Y. L. Wang, T. Liang and C. J. Cheng, A novel ion-responsive photonic hydrogel sensor for portable visual detection and timely removal of lead ions in water, *Mater. Adv.*, 2022, **3**(13), 5393–5405.
10 S. H. Yap, Y. H. Chien, R. Tan, A. R. bin Shaik Alauddin, W. B. Ji, S. C. Tjin and K. T. Yong, An advanced hand-held microfiber-based sensor for ultrasensitive lead ion detection, *ACS Sens.*, 2018, **3**(12), 2506–2512.
11 N. Yildirim, F. Long, M. He, C. Gao, H. C. Shi and A. Z. Gu, A portable DNAzyme-based optical biosensor for highly sensitive and selective detection of lead (II) in water sample, *Talanta*, 2014(129), 617–622.
12 G. Zhou, J. Chang, S. Cui, H. Pu, Z. Wen and J. Chen, Real-time, selective detection of Pb2+ in water using a reduced graphene oxide/gold nanoparticle field-effect transistor device, *ACS Appl. Mater. Interfaces*, 2014, **6**(21), 19235–19241.
13 Y. Li, C. Wang, Y. Zhu, X. Zhou, Y. Xiang, M. He and S. Zeng, Fully integrated graphene electronic biosensor for label-free detection of lead (II) ion based on G-quadruplex structure-switching, *Biosens. Bioelectron.*, 2017, **89**, 758–763.
14 A. Maity, X. Sui, C. R. Tarman, H. Pu, J. Chang, G. Zhou, R. Ren, S. Mao and J. Chen, Pulse-driven capacitive lead ion detection with reduced graphene oxide field-effect transistor integrated with an analyzing device for rapid water quality monitoring, *ACS Sens.*, 2017, **2**(11), 1653–1661.
15 X. Sui, H. Pu, A. Maity, J. Chang, B. Jin, G. Lu, Y. Wang, R. Ren, S. Mao and J. Chen, Field-effect transistor based on percolation network of reduced graphene oxide for real-time ppb-level detection of lead ions in water, *ECS J. Solid State Sci. Technol.*, 2020, **9**(11), 115012.
16 S. A. Pullano, C. D. Critello, I. Mahbub, N. T. Tasneem, S. Shamsir, S. K. Islam, M. Greco and A. S. Fiorillo, EGFET-based sensors for bioanalytical applications: A review, *Sensors*, 2018, **18**(11), 4042.
17 J. Kwon, B. H. Lee, S. Y. Kim, J. Y. Park, H. Bae, Y. K. Choi and J. H. Ahn, Nanoscale FET-based transduction toward sensitive extended-gate biosensors, *ACS Sens.*, 2019, **4**(6), 1724–1729.
18 H. J. Jang, X. Sui, W. Zhuang, X. Huang, M. Chen, X. Cai, Y. Wang, B. Ryu, H. Pu, N. Ankenbruck and K. Beavis, Remote floating-gate field-effect transistor with 2-dimensional reduced graphene oxide sensing layer for reliable detection of SARS-CoV-2 spike proteins, *ACS Appl. Mater. Interfaces*, 2022, **14**(21), 24187–24196.
19 H. J. Jang, W. Zhuang, X. Sui, B. Ryu, X. Huang, M. Chen, X. Cai, H. Pu, K. Beavis, J. Huang and J. Chen, Rapid, sensitive, label-free electrical detection of SARS-CoV-2 in nasal swab samples, *ACS Appl. Mater. Interfaces*, 2023, **15**(12), 15195–15202.
20 A. Nag, A. Mitra and S. C. Mukhopadhyay, Graphene and its sensor-based applications: A review, *Sens. Actuators, A*, 2018, **270**, 177–194.
21 F. Yavari and N. Koratkar, Graphene-based chemical sensors, *J. Phys. Chem. Lett.*, 2012, **3**(13), 1746–1753.
22 E. B. Secor, P. L. Prabhumirashi, K. Puntambekar, M. L. Geier and M. C. Hersam, Inkjet printing of high conductivity, flexible graphene patterns, *J. Phys. Chem. Lett.*, 2013, **4**(8), 1347–1351.
23 Z. Gao, L. Wang, X. Huang, C. Benmore, H. Pu, J. Wen, W. Zhuang, M. K. Chan and J. Chen, Selective single-atom adsorption for precision separation of lead ions in tap water via capacitive deionization, *Water Res.*, 2025, **268**, 122665.
24 C. Wang, H. Pu, X. Sui, S. Zhou and J. Chen, Hybrid modeling and sensitivity analysis on reduced graphene oxide field-effect transistor, *IEEE Trans. Nanotechnol.*, 2021, **20**, 404–416.
25 N. Kong, X. Huang, L. Cui and J. Liu, Surface modified graphene for heavy metal ions adsorption, *Sci. Adv. Mater.*, 2013, **5**(8), 1083–1089.
26 R. Say, A. Denizli and M. Y. Arıca, Biosorption of cadmium (II), lead (II) and copper (II) with the filamentous fungus Phanerochaete chrysosporium, *Bioresour. Technol.*, 2001, **76**(1), 67–70.
27 W. Zhuang, H. J. Jang, X. Sui, B. Ryu, Y. Wang, H. Pu and J. Chen, Enhancing Electrochemical Sensing through Molecular Engineering of Reduced Graphene Oxide–Solution Interfaces and Remote Floating-Gate FET Analysis, *ACS Appl. Mater. Interfaces*, 2024, **16**, 27961–27968.
28 S. Baachaoui, S. Aldulaijan, L. Sementa, A. Fortunelli, A. Dhouib and N. Raouafi, Density functional theory investigation of graphene functionalization with activated carbenes and its application in the sensing of heavy metallic cations, *J. Phys. Chem. C*, 2021, **125**(48), 26418–26428.